
IDENTIFYING AUTISM SPECTRUM DISORDER BASED ON INDIVIDUAL-AWARE DOWN-SAMPLING AND MULTI-MODAL LEARNING

A PREPRINT

Li Pan¹, Jundong Liu², Mingqin Shi³, Chi Wah Wong⁴, and Kei Hang Katie Chan^{1,2,5}

¹Department of Electrical Engineering, City University of Hong Kong, Hong Kong SAR

²Department of Biomedical Sciences, City University of Hong Kong, Hong Kong SAR

³School of Basic Medical Sciences, Yunnan University of Chinese Medicine, Kunming, China

⁴Department of Applied AI and Data Science, City of Hope, Duarte CA 91010, USA

⁵Department of Epidemiology, Brown University, Providence RI 02912, USA

ABSTRACT

Autism Spectrum Disorder(ASD) is a set of neurodevelopmental conditions that affect patients' social abilities. In recent years, many studies have employed deep learning to diagnose this brain dysfunction through functional MRI (fMRI). However, existing approaches solely focused on the abnormal brain functional connections but ignored the impact of regional activities. Due to this biased prior knowledge, previous diagnosis models suffered from inter-site heterogeneity and inter-individual phenotypic differences. To address this issue, we propose a novel feature extraction method for fMRI that can learn a personalized lower-resolution representation of the entire brain networking regarding both the functional connections and regional activities. Specifically, we abstract the brain imaging as a graph structure and straightforwardly downsample it to sparse substructures by hierarchical graph pooling. The down-scaled feature vectors are embedded into a population graph where the hidden inter-subject heterogeneity and homogeneity are explicitly expressed as inter- and intra-community connectivity differences. Subsequently, we fuse the imaging and non-imaging information by graph convolutional networks (GCN), which recalibrates features to node embeddings under phenotypic statistics. By these means, our framework can extract features directly and efficiently from the entire fMRI and be aware of implicit inter-individual variance. We have evaluated our framework on the ABIDE-I dataset with 10-fold cross-validation. The present model has achieved a mean classification accuracy of 85.95% and a mean AUC of 0.92, better than the state-of-the-art methods. Our code and support documents are available at github.com/jhonP-Li/ASD_GP_GCIN

Keywords ABIDE · Autism Spectrum Disorder · Graph Convolutional Networks · Graph Pooling

1 Introduction

Autism spectrum disorder (ASD), a range of brain developmental disorders, has commonly been reported worldwide. In 2020, a survey found that approximately 1 in 45 children in the U.S. was diagnosed with this disease caused by genetic and environmental factors[1]. This mental disorganization, which will result in difficulties with social interaction and communication, can be noticed at the early age of a child. However, another study, done in the U.K., showed that the time-consuming current diagnosis process could cause a delay of around 3.5 years from the point at which parents first consult a doctor to the confirmation of an ASD diagnosis[2], which results in unnecessary panic and late intervention.

Similar to physical disease diagnosis, this brain dysfunction can be detected with pathological manifestations. In [3], the authors proposed a diagnosis method based on the MRI. It was discovered that there existed structural differences in some certain areas between patients and typical control subjects. [4] reported abnormal brain function connections found on ASD subjects. However, these diagnosis methods are too complex and specific to be promoted as general ones. In recent years, brain imaging analysis based on deep learning and machine learning has been widely studied.

[5] employed Long Short-Term Memory (LSTM) to analyze the time-series data of fMRI automatically. [6] applied Deep Neural Networks (DNN) directly on the fMRI and reported the performance improvement compared to Support Vector Machine (SVM) and Random Forest (RF). In [7], the authors designed a Convolutional Neural Networks (CNN) architecture with fMRI as input and achieved slightly better performance than the DNN did. [8] reached the best performance of end-to-end CNN models by 3D-CNN and ensemble brain atlas.

Limited by the number of available training data samples and the high complexity of fMRI, the naive end-to-end implementation of CNN models has reached the bottleneck. On the one side, the functional connections of brain regions do not follow the spatial distributions of them, e.g., a node may interact with another far away from it [9]. However, the convolution kernels can only extract features from spatial neighborhoods for each pixel. To be aware of those cross-space connections, CNN needs more convolution layers to form a wider receptive field, which backfires to overfitting due to the lack of samples. On the other side, to downsample the raw inputs, many methods have focused on selecting a certain number of functional connections. These methods represent brain imaging as a correlation coefficient matrix of which the elements denote the covariances between every two regions based on their time-series signals. For example, in [10], the authors found the impact of the brain functional connections in this disease predicting problem. and suggested 26.4 million possibilities of them. [11] extended the previous work by selecting the best framework from different brain atlases and regional correlation computing methods. [12] directly downsampled the raw functional connections into the low-dimensional space by Principle Component Analysis (PCA). Yet, this straightforward dimension reduction method achieved even worse performance than the end-to-end models owing to the lack of samples. [13] reported the state-of-the-art performance by quantifying inter-site measurement variances. However, the elaborate task-specific feature selection workflow is hard to generalize to other brain imaging downsampling problems. [9] compared two feature selection models, autoencoder and Multilayer Perceptron(MLP), which both can automatically extract features from the raw inputs. [14, 15] enhanced it with deep feature representation and multi-task feature selection, respectively. In a word, all the feature selection methods mentioned above solely extract features from the pairwise regional correlation matrix. This inflexible Euclidean representation of brain imaging did not only ignore the details of regional signals, which are also believed to relate to ASD [16, 17, 18, 19], but also omit the latent interaction among the connections.

On the contrary, we describe brain imaging as a graph structure, which perspicuously expresses the functional interactivity among regions as edges among nodes. Compared to the above brain modeling methods, this geometric form globally organizes brain regions and their connections. [20] constructed a personalized brain connectivity graph for each individual and compared every graph structure by graph convolutional networks, which reached a lower classification accuracy compared to CNN models due to the under-learned graph difference metrics. [21] utilized graph convolutional networks on the geometric representation of the brain and tried to interpret the learned connections as ASD biomarkers. To efficiently extract features from this non-Euclidean structure, we have exploited graph pooling which can directly learn those cross-space connections. For example, the intuitive pooling methods straightforwardly summed up or averaged all the node embeddings at the final layer [22]. In [23], the authors manipulated topK node selection and graph convolutional networks to learn a group-level substructure. But that strategy has ignored the possible variance among individuals, and the selected subgraphs are not sufficient to be paraphrased as biomarkers considering the limited size of the dataset and classification accuracy.

In the context of this ASD disease prediction problem, another challenge is the non-imaging difference between individuals, i.e., gender, handedness, IQ, etc. Though this information is not present in the fMRI, it does affect the probability of suffering from ASD. For example, [24] indicated that One in every 42 males and one in 189 females in the United States is diagnosed with an autism spectrum disorder. [25] reported the correlation between the handedness and ASD. Besides, the fMRI scanning devices and measurement parameters from different data collection sites are not strictly the same [13]. Those hidden factors have caused the non-identity distribution of features and lowered the generalization ability of models. To address this, some authors manually forced those settings to be the same. For example, in [26, 27, 28, 29], the authors elaborately chosen training and testing samples from a certain data collection site. Hence, the implicit differences among samples were further narrowed, and these methods achieved much better classification performance than the models evaluated on the entire dataset. Although this hard clustering strategy did prove the feasibility of ASD diagnosis based on deep learning, the generalization ability of the models cannot be guaranteed as the number of samples has been dramatically reduced in that way.

To address the above issue, we employ Graph Convolutional Networks (GCN) to recalibrate the features extracted from brain imaging, according to the non-imaging data. Unlike assigning each subject into a cluster, we embed each subject into a population graph, where nodes denote individuals and edges represent the phenotypic similarity between every two nodes. Thus, the hidden inter-subject heterogeneity and homogeneity are explicitly expressed as inter- and intra-community connectivity differences. Initially, the nodes are associated with features extracted from the graph representation of brain imaging. Then, the GCN, which extends the convolution operations to non-Euclidean data structures, is employed on the whole population graph. At each layer, the GCN block represents the node features as the weighted sum of the features of neighbors. With the derived node embeddings, the characteristics of individuals in

Table 1: Overview of the ABIDE I dataset preprocessed by CPAC

Sites	Age(year)		Gender		handedness				Diagnostic group	
	Min	Max	Male	Female	Left	Right	Ambi*	Mixed	ASD	Control
CALTECH	17.0	56.2	10	5	1	13	1	0	5	10
CMU	19.0	33.0	7	4	1	10	0	0	6	5
KKI	8.2	12.8	24	9	1	27	0	5	12	21
LEUVEN	12.1	32.0	49	7	7	49	0	0	26	30
MAX_MUN	7.0	58.0	42	4	2	44	0	0	19	27
NYU	6.5	39.1	136	36			N/A		74	98
OHSU	8.0	15.2	25	0	1	24	0	0	12	13
OLIN	10.0	24.0	23	5	5	23	0	0	14	14
PITT†	9.3	35.2	43	7	4	45	0	0	24	26
SBL†	20.0	49.0	26	0	1	0	0	0	12	14
SDSU	8.7	17.2	21	6	2	25	0	0	8	19
STANFORD	7.5	12.9	18	7	3	20	2	0	12	13
TRINITY	12.0	25.7	44	0	0	44	0	0	19	25
UCLA	8.4	17.9	74	11	9	76	0	0	48	37
UM†	8.2	28.8	93	27	15	97	0	0	47	73
USM	8.8	50.2	67	0			N/A		43	24
YALE	7.0	17.8	25	16	7	34	0	0	22	19
Total	6.5	58.0	727	144	59	531	3	5	403	468

* Ambi: Ambidextrous

† The handedness information of some subjects is unavailable.

the same community become more similar, and the inter-community feature distribution becomes more different. In other words, the node features extracted from brain imaging are further recalibrated according to the inter-individual phenotypic variance. In [30], the authors employed GCN on the population graph for the first time and achieved performance improvement compared to end-to-end one-stage classifiers by leveraging imaging and non-imaging information. [31] extended the previous work by fusing both the MRI and fMRI into node features of the population graph. [32] tried to embed the linear graph convolution of brain graph modeling into the population graph. But both resulted in a lower accuracy owing to the increased model complexity.

In this study, we propose a novel framework that incorporates graph pooling and graph convolutional networks. We explicit graph pooling to downsample the non-Euclidean form of brain imaging, whereas previous brain modeling methods can solely extract features from functional connections. The individually selected brain substructures, which are flattened and then further regularized under inter-subject hidden factors to node embeddings, preserve node-and-edge information and are clustering-like distributed in terms of phenotypic data. Having merged functional connections, regional activities, and non-imaging data, our framework presents its superior in ASD diagnosis, reaching an accuracy of 85.95% on ABIDE I dataset. The main contributions of our work are four-fold:

- 1) We have employed a novel feature extraction method on fMRI feature extraction tasks. The unsupervised graph pooling efficiently extracts features from the non-Euclidean brain networking. By weighing both the functional connections and regional signals simultaneously, this efficient feature extractor has achieved promising performance in identifying brain disorders even with a linear classifier.
- 2) We have fused the multi-modal information through graph convolutional networks and intuitively illustrated its efficiency. This step successfully further stabilized the model classification performance by recalibrating extracted features according to non-imaging information.
- 3) Different from hard selecting universal biomarkers of ASD, our framework tends to select a personalized substructure of brain networking for each individual. This novel strategy has detected inter-group heterogeneity and intra-group homogeneity regarding brain activities.
- 4) We have constructed an ASD diagnosing framework, which outperforms state-of-the-art methods on the ABIDE I dataset, reaching a classification accuracy of 85.95% and AUC of 0.92. This clinically meaningful automatic ASD identification method could contribute to early detection and intervention for this brain disorder.

The rest of the paper is organized as follows: Section II introduces the datasets and illustrates the details of the proposed model. In Section III, we present the experimental setup, evaluation metrics, experimental results and comparison

with other methods, ablation study, and intuitive exhibition of model mechanisms. Finally, we draw the conclusion in Section IV.

2 Materials and Methods

2.1 ABIDE Dataset

Constructed by [33], the ABIDE I dataset contains a variety of information of 1,112 subjects, i.e., MRI, fMRI, and phenotype data, collected from 17 international sites. To reduce the fMRI measurement error, current studies are focusing on the preprocessed data. [34] performed four different preprocessing pipelines on the original material. To compare with other methods [9, 13, 6, 8, 10], in the current paper, we have used the data preprocessed by the Configurable Pipeline for the Analysis of Connectomes (CPAC). Built by [34], the chosen functional preprocessing pipeline includes time slicing, motion correction, skull-stripping, global mean intensity normalization, and nuisance signal regression. Thus, the noise caused by unrelated motions, like the heart beating, is reduced. To further regularize the input sample features, we have also employed band-pass filtering and global signal regression.

As shown in the table 1, the processed data contains 403 ASD subjects and 468 typical control subjects. Caused by the measurement difference among different sites, some categories of the phenotype data are not or partially collected, like handedness information. Moreover, the distribution of the dataset is unbalanced on some features. For example, the 17 sites only have collected 144 female samples but collected 727 male samples. According to the view of [24], gender is a rather important factor affecting the probability of ASD. This unbalanced feature distribution, which is not present in the MRI or fMRI data, has caused the non-identical distribution of features and thus affected the performance of unimodal learning models.

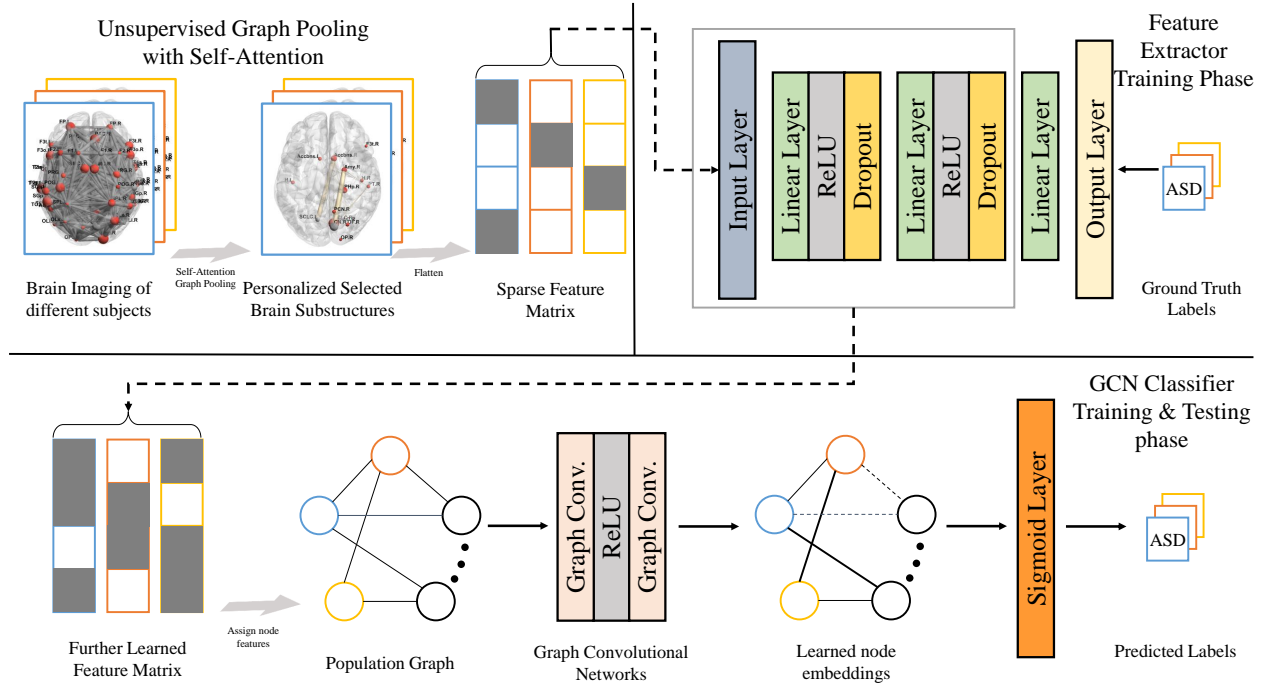


Figure 1: Overview of the proposed framework; The top-left part illustrates self-attention graph pooling in section 2.3. The top-right part indicates the training phase of feature extractor, where we train the MLP using the pooling output. In the bottom part, we construct a population graph, where nodes denote subjects and edges represent interindividual phenotypic similarity. We then train a GCN model by assigning each node with dense features extracted by MLP.

To further reduce the dimensionality of input data, fMRI is separated logically as signals of regions of interest (ROIs). The voxel-wise time series is thus paraphrased as the time series of regional signals. Proposed by [35, 36, 37, 38], the Harvard-Oxford atlas is split into cortical and subcortical structural probabilistic atlases. The HO atlas, which has also been selected by other works [8, 9, 6], is filtered with a 25% threshold and subsequently divided into left and right hemispheres at the midline. The ROIs represent 110 functional brain regions, i.e., left and right Hippocampus, left and

right Cuneal Cortex, left and right Planum Temporale, left and right Occipital Pole, etc. Thus, the original 4D brain imaging is further downsampled to a 2D data structure, containing 110 regions and the corresponding time series for each area.

2.2 Model Overview

As shown in the figure 1, the whole pipeline consists of three main parts. First, the unsupervised graph pooling directly downsamples the graph representation of the brain to a sparse brain networking. We then train a multilayer perception using the flattened features and ground truth labels. Finally, we employ a two-layer graph convolutional network to learn the node embeddings by embedding every individual into the population graph and building edges according to the phenotypic information.

2.3 Graph Pooling

In this section, we implement the Hierarchical Graph Pooling with Structural Learning presented by [39] to extract the features from the fMRI. It improves the existing brain imaging feature extractors in two main aspects. First, it can extract features directly from the entire graph structure, while other methods only extract features from functional connections. Second, this graph pooling operation downsamples graph without supervision. In other words, this step can be directly added to other related frameworks without any additional training cost. Graph pooling, as a downsampling method for graph structure, is a central component of graph convolutional networks in graph classification tasks. For example, the intuitive idea is to average all node embeddings to represent the entire graph[22]. Compared to other graph pooling methods[40, 41], the Hierarchical Graph Pooling with Structural Learning is designed to preserve the information and connectivity of the graph and reduce the information redundancy. Having achieved state-of-the-art performance on graph classification problems, this method efficiently extracts the data from the non-Euclidean form of brain imaging.

Before this implementation of graph pooling, other models trained classifiers, like MLP, or constructed a specific feature extracting framework to extract features from the functional connections[9, 14, 15, 13] which are represented as the correlation coefficients of every two regions. At this phase, those methods have directly ignored the details of regional brain activities. This intuitive method, mapping the two vectors to a float ranging from -1 to 1, has reduced the data complexity. However, this edge-only feature extraction strategy has caused much more information loss to the entire graph structure regarding the time series of brain regions as node features and functional connections as edges. Moreover, studies have proved the importance of the node features in the diagnosis of ASD. In [16, 17, 18, 19], the authors reported the abnormal regional activities among ASD subjects. Thus, leveraging the information of both functional connections and regional activities, graph pooling has proved its superior in this brain disorder diagnosis as shown in section 3.3.

2.3.1 Graph Representation of Brain Imaging

After being labeled as 110 regions according to the HO atlases, fMRI can be abstracted as a graph structure, where nodes denote brain regions and edges indicate functional connections. Initially, every node is assigned with a feature vector that represents the time series of regional activity. In [9], the authors defined 6105 brain functional connections by connecting right-side regions to the left side and left-side regions to the right. Inspired by it, we construct a graph representation of brain imaging, where regions are connected according to the same strategy and all regions are connected with the global mean time series to reduce measurement error further. In short, the input graph representation of brain imaging containing 111 nodes, 110 for the brain regions and 1 for the fMRI global mean signal, and 6215 edges.

2.3.2 Node Selection

The hierarchical graph pooling consists of two parts: First, it selects the nodes based on the criterion of minimizing graph information loss. Subsequently, to connect the probably isolated subgraph caused by the node selection and recorrect the initial brain regional connections to some degree, the edge prediction method is employed between the two-hop neighbors of each node and itself. At the first component, a node information score is defined as the absolute value of the Manhattan distance between the node features itself and the one constructed from its neighbors:

$$S = \gamma(g) = \left\| (I - (D^{(l)})^{-1}A^{(l)})H^{(l)} \right\|_1 \quad (1)$$

where $A^{(l)}$ and $H^{(l)}$ are the adjacency and node features matrices of the l -th layer. The information of edges is present implicitly as the connections among nodes. I represents the identity matrix and $D^{(l)}$ denotes the l -th layer diagonal

degree matrix of $A^{(l)}$. $\|\cdot\|_1$ performs the \mathcal{L}_1 norm row-wisely. The vector S contains the information score of each node, which indicates its importance at this selection stage. The nodes are then selected by ranking and selecting the top-K ones regarding the information score:

$$\begin{aligned} idx &= \text{top}(S, \lceil r * n^{(l)} \rceil) \\ H^{(l+1)} &= H^{(l)}(idx, :) \\ A^{(l+1)} &= A^{(l)}(idx, idx) \end{aligned} \quad (2)$$

where r is the pooling ratio which is set manually and will be discussed in the section 3.3. The function $\text{top}(\cdot)$ returns the indices of top $n^{(l+1)} = \lceil r * n^{(l)} \rceil$ values of the information scores S . $H^{(l)}(idx, :)$ and $A^{(l)}(idx, idx)$ performs the element selection according to the indices of top information scores. Thus, in the l -th layer, $n^{(l+1)}$ nodes are remained and others are removed.

Intuitively, the information score of a node is the feature difference between the average value of its neighbors and itself. The greater the difference, the higher the information score, and the less likely to remove the node. For example, if the feature of a node is equal to the average feature of its neighbors, it may be safe to drop this node without further information loss to the entire graph. On the other side, this selection method simulates a probable universal strategy for removing the information redundancy of fMRI: If the blood oxygen level activity is close to its neighbors, the area may be regarded as coactivated with its neighbors. After Removing all those nodes, the remaining ones may be activated in the first order, which may act like a trigger that has launched the sequence of regional brain activities.

2.3.3 Edge Prediction

At the same time, the node selection method may isolate some subgraphs and be sensitive to the initialization of brain graph structure, as it can not learn new connections beyond the given ones. To preserve the completeness of the graph, [39] developed a structural learning method that learned sparse graph structure through a sparse attention mechanism. Proposed by [42], the underlying pairwise relationship between disconnected nodes can be represented as the following:

$$\sigma^{(l)}(p, q) = \text{ReLU}(\vec{\alpha}[H^{(l)}(p, :)||H^{(l)}(q, :)]^T) \quad (3)$$

where $H^{(l)}$ represents the feature matrix at the l -th layer. Thus, a similarity-like value is learned through the features of the two nodes. By adding a bias factor to keep a relatively large similarity to the connected nodes, the similarity score between two nodes can be measured as the follows:

$$\begin{aligned} E^{(l)}(p, q) &= \sigma^{(l)}(p, q) + \lambda \cdot A^{(l)}(p, q) \\ \text{Sim}^{(l)}(p, q) &= \frac{\exp(E^{(l)}(p, q))}{\sum_{m=1}^{n^{(l)}} \exp(E^{(l)}(p, m))} \end{aligned} \quad (4)$$

where $E^{(l)}(p, q)$ is the similarity score between the two nodes calculated by the attention mechanism. The bias $\lambda \cdot A^{(l)}(p, q)$ assigned a relatively larger similarity score to the directly connected nodes. With normalized similarity values $\text{Sim}^{(l)}(p, q)$, this mechanism succeeded in predicting the possible edges between disconnected nodes. Thus, the connectivity of the pooled graph can be preserved. Moreover, as shown in figure 4, this step is able to predict some connections that are not given in the initialization step, which makes the model more robust.

After three layers of graph pooling, the raw graph is downsampled to the sum-up of the three different hierarchical representations. The pooling output is then flattened and fed into a multilayer perception. At the training stage, we have employed a particular procedure, i.e., we have run another 10-fold cross-validation on the given training folds and chosen the model that has been trained for at least 100 epochs and achieved the highest accuracy on the validation set to avoid overfitting and underfitting. After training, we remove the final linear layer and select the output feature map of the other two layers as the learned features, which will be discussed in section 2.4.

2.3.4 Personalized Feature Extraction

To conclude a universal ASD clinical diagnosis suggestion, [9, 14, 15, 13] tried to manually select top-N critical functional connections from the fMRI of all subjects. Ideally, this procedure would return some functional connections from which we could quickly tell if someone is suffering from this brain disorder. However, as discussed in [9], the results are not satisfactory: The highest mean accuracy is 70.40%, and the smallest number of selected functional connections is 250, which is not adequate nor efficient for clinical diagnosis.

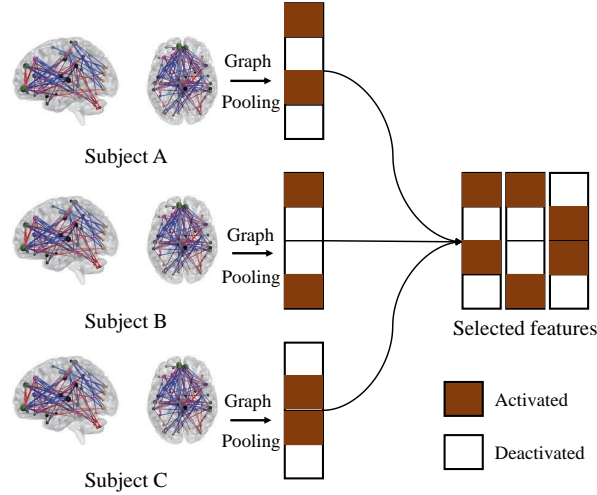


Figure 2: Illustration of sparse feature fusion in graph pooling

Different from that ambitious universal key features selection, we develop a personalized feature extraction strategy. Instead of selecting a set of universal biomarkers of ASD, we treat each subject separately and downsample the graph modeling according to its characters. As illustrated in the figure 2, we performed graph pooling onto every individual and stored the results as sparse vectors. In terms of storage and computation cost, that strategy has successfully downsampled the input brain imaging like the above hard selection. On the other hand, the feature matrix has preserved more information than the previous methods. The two main benefits of this sparse feature fusion are as follows: First, it downsamples the brain imaging to extraordinarily few key components even without a performance decrease, which will be discussed in the section 3.3. Second, the difference in selected features between individuals has clinical meanings. It may indicate the varied brain regional activities and connections among different groups and will be discussed in the section 3.4.

2.4 Graph Convolutional Networks

To fuse brain imaging data and non-imaging data, we constructed a population graph where nodes represent subjects and edges indicate the similarity degree regarding phenotypic information. The non-imaging information similarity among subjects is characterized as the connectivity degree among nodes, i.e., nodes with similar phenotypic properties are more likely to be in the same community. We employ Graph Convolutional Networks to process the population graph structure with every node associated with a feature vector extracted from brain imaging by graph pooling. Proposed by [43], GCN extends convolution operations onto graph structures and is able to extract higher-order features from node embeddings. At each layer of GCN, the node feature vector is then recalculated as the lower-dimensional weighted sum of its and its neighbors' features, that is, the node embedding. Hence, the features of nodes that are in the same community tend to follow a similar distribution. A logistic regression classifier is trained on the last node features to predict the labels of each subject.

2.4.1 Population Graph Construction

As stated in section 2.1, we use the data of 871 subjects preprocessed by CPAC. The connection between two nodes is decided by their phenotypic similarity, i.e., gender, age, handedness, etc. However, caused by inconsistent measurement among different data collection sites, some categories of data are not or partly collected. For example, nearly 30% of the handedness data are not available as illustrated in the table 1. Suggested by [9], we consider a subset of the whole non-imaging data, which contains gender, age, and data collection sites information. Intuitively, the similarity is computed as the cosine similarity between two phenotypic feature vectors M_u and M_v .

$$Sim(u, v) = \frac{M_u \cdot M_v}{\|M_u\| \|M_v\|} \quad (5)$$

Table 2: Comparison with state-of-the-art methods on ABIDE I dataset

References	Methods	Performance		
		Accuracy	Sensitivity	Specificity
[30]	GCN	69.50	-	-
[5]	LSTM	66.80	-	-
[11]	SVC	66.80	61.00	72.30
[6]	DNN	70.00	74.00	63.00
[9]	MLP and GCN	70.40	-	-
[8]	3D-CNN	73.30	-	-
[45]	Autoencoder	67.50	68.30	72.20
[13]	FCs selection and LDA	77.70	-	-
[46]	Joint learning	73.10	71.40	74.60
[7]	CNN	70.20	77.00	61.00
[15]	FCs selection and SVM	76.80	72.50	79.90
[14]	FCs selection and MLP	74.52	80.69	66.71
Present study	Graph pooling and LR	84.54	83.48	86.75
	Graph pooling and GCN	85.95	83.62	87.82

GCN: Graph Convolutional Networks
LSTM: Long Short-Term Memory
SVC: Support Vector Classification
MLP: Multi-Layer Perceptron
LDA: Linear Discriminant Analysis
LR: Logistic Regression
FCs: Functional Connections

where $M = \{Age, Gender, Site\}$ denotes the selected subset of non-imaging data. A threshold of 0.5 is then applied to the derived similarity values to decide whether the two nodes u, v are connected or not.

$$A(u, v) = \begin{cases} 1, & \text{if } Sim(u, v) > 0.5 \\ 0, & \text{otherwise} \end{cases} \quad (6)$$

where $Sim(u, v)$ is the similarity score of the two subjects. A represents the adjacency matrix of the graph. Two nodes are connected if their cosine similarity value is above 0.5. By these means, the population graph is initialized as an undirected graph containing 871 nodes.

2.4.2 GCNs

We have implemented two kinds of GCN in this part. The first layer is the same as the one proposed by [43]. The second layer is the Cluster-GCN presented by [44], which has accelerated the basic GCN block.

Extending convolution operations to non-Euclidean space, GCNs have achieved promising performance on arbitrarily structured graphs. Though there exist different forms of GCN block, the universal core task is to learn a non-linear function $f(H^{(l)}, A)$ which aggregates the feature vectors of connected nodes to generate features for next layer:

$$H^{(l+1)} = f(H^{(l)}, A) = \sigma(\tilde{D}^{-\frac{1}{2}} \tilde{A} \tilde{D}^{-\frac{1}{2}} H^{(l)} W^{(l)}) \quad (7)$$

with $\tilde{A} = A + I$, where I is the identity matrix and \tilde{D} is the diagonal node degree matrix of \tilde{A} . For the l -th layer of the GCN, the graph can be represented as the feature matrix $H^{(l)}$. $H^{(0)} = X$ and $H^{(L)} = Z$ denote the input and final output feature matrix respectively. $W^{(l)}$ is the learnable weight matrix and $\sigma(\cdot)$ is the non-linear activation function, ReLU. In this way, the features are aggregated to form features of the next layer. [44] reduced the computational cost by clustering nodes into multiple batches:

$$\frac{1}{|\mathcal{B}|} \sum_{i \in \mathcal{B}} \nabla loss(y_i, z_i^L) \quad (8)$$

where \mathcal{B} indicates the subset of nodes and z_i^L represents the final prediction label of the i -th subject. Hence, at the loss back-propagation phase, the model only needs to calculate the gradient for the mini-batch. The Binary Cross-Entropy Loss is defined as the loss function:

$$\text{loss}(y_i, z_i^L) = -[y_i * \log(z_i^L) + (1 - y_i) * \log(1 - z_i^L)] \quad (9)$$

After the graph convolutional layers, a linear classifier is applied on each node. The final outputs of the classifier represent the probability of ASD. By filtering the probabilities with a 0.5 threshold, the model finally outputs the predicted diagnostic group of each subject.

3 Experimental analysis

3.1 Experimental Settings

To make this experiment consistent with other studies [8, 13, 7, 9, 30, 5], we have performed the 10-fold cross-validation on the 871 samples and repeated it ten times. The multilayer perceptron and graph convolutional network are trained separately but strictly on the same train set. At the training stage of multilayer perceptron, we have run another 10-fold cross-validation on each given training fold to ensure the generalization of the extracted features. The whole framework is trained and tested on an NVIDIA TESLA V100S. During the optimization, we have utilized the Adam optimizer, of which the parameters are as follows: learning rate = 0.0001, weight decay = 0.01. We have also used the dropout to enhance the generalization of GCN with a dropout ratio of 0.01.

3.2 Results

In the table 2, we have compared our framework with other models on the same ABIDE I dataset preprocessed by CPAC [34]. In general, those methods can be categorized into two types: single-stage and multi-stage. The single-stage methods directly deploy deep learning methods, like CNN, to deal with this ASD VS Control binary image classification problem[5, 11, 6, 8, 45, 7]. However, limited by the number of available training samples, these naive implementations of neural networks have not achieved better performance for years. On the other hand, multi-stage methods usually consist of two components: feature extraction and classification. Previous works trained feature extractors to extract features from brain functional connections[9, 13, 15, 14]. A classifier, like SVC, is then trained with extracted features as inputs. This kind of framework has successfully downsampled the high-dimensional brain imaging and thus made obvious performance improvement even with linear classifiers compared to the straightforward CNN models. For example, [13] constructed a specific workflow to select the key features from brain imaging and achieved an accuracy of 77.7% with linear discriminant analysis.

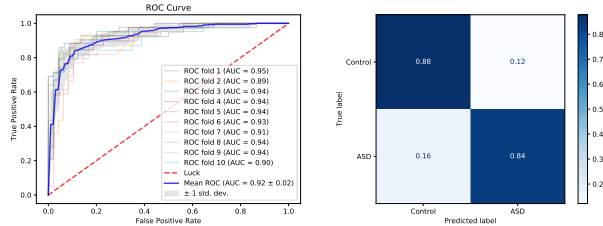


Figure 3: Performance of the present model, Graph pooling and GCN, on ABIDE I dataset: the ROC curve and confusion matrix

Like the above multi-stage methods, the present framework includes feature extraction and classification parts. We have employed graph pooling to downsample the given brain networking and trained a multilayer perceptron to further extract features, whereas previous feature extractors can only extract features from functional connections. Inspired by [9], we employ GCN in the final classification part, which has leveraged imaging and non-imaging information. By these means, our framework outperforms the state-of-the-art method, reaching an accuracy of 85.95% and a mean AUC of 0.92. The efficiency of graph pooling is discussed in the following part.

3.3 Efficiency of Graph Pooling

As previously mentioned, studies have reported abnormal brain functional connections found on ASD subjects[4]. With this prior knowledge, in [9, 13, 15, 14], the authors only simplified brain imaging as functional connections. Specifically,

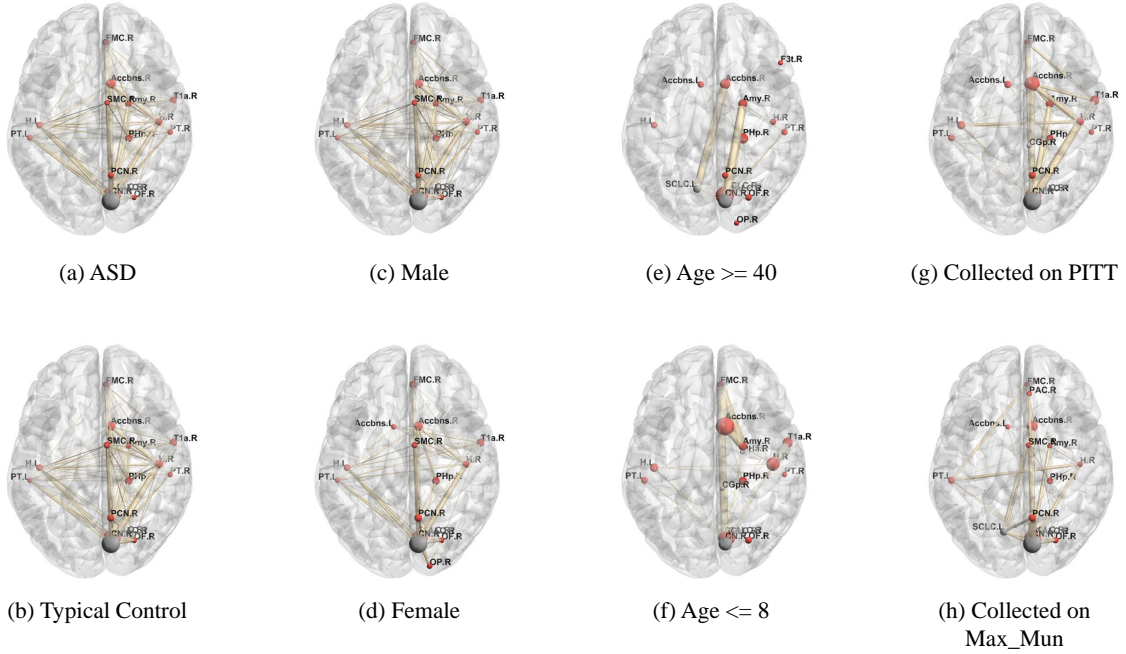


Figure 4: Result of graph pooling for different groups. The pooling ratio is set as 0.05, i.e., 6 regions are selected out of 111. Each axial view of the brain shows the top 15 nodes most frequently selected from those who are inside the corresponding group. The width of edges and size of nodes indicate the relative frequency of being selected. Number of subjects inside each group are as follows: a: 403; b: 468; c: 727; d: 144; e: 14; f: 15; g: 50; h: 46.

they computed correlation coefficients between every two regions and fed them into feature extractors. This correlation coefficient matrix representation of the brain successfully downsampled raw fMRI data, whereas it also resulted in crucial information loss as the regional features were omitted. In contrast, graph pooling extracts features directly from the graph representation of the brain. As shown in the table 3, graph pooling has outperformed the state-of-the-state method, reaching an accuracy of 84.54% even with linear regression as a classifier. Especially, in [11], the authors have developed a similar workflow and achieved an accuracy of 66.80%. The only difference is that they extracted features from functional connections, whereas graph pooling downsamples the brain graph representation.

Table 3: The accuracy of ABIDE I classification with linear classifiers for different feature extraction methods

References	Feature extractor and classifier	Accuracy
[10]	FCs and SVC	60.00
[11]	MLP and SVC	66.80
[14]	FCs selection and MLP	74.52
[15]	FCs selection and SVM	76.80
Present study	Graph pooling and LR	84.54

To further evaluate the efficiency of graph pooling, we have tested the graph pooling progress for different values of the pooling ratio. Previous functional connection selection methods chose a certain number of edges from the graph representation of the brain[9, 13]. That inflexible strategy disregarded the heterogeneity of brain activities caused by inter-individual differences and even occasional personal status. Thus, that static procedure failed to achieve a satisfactory classification performance. As previously discussed in section 2.3.4, the self-attention mechanism inside graph pooling has realized personalized brain essential components selections. Illustrated in figure 5, the classification of the framework is not sensitive to the super parameter, pooling ratio. The highest accuracy is even achieved with a pooling ratio of 0.005.

The main advantages of graph pooling are 3-fold: First, it can be easily generalized to other related problems. Previous methods work under a strong assumption that it is only the abnormal functional connections that cause ASD. This

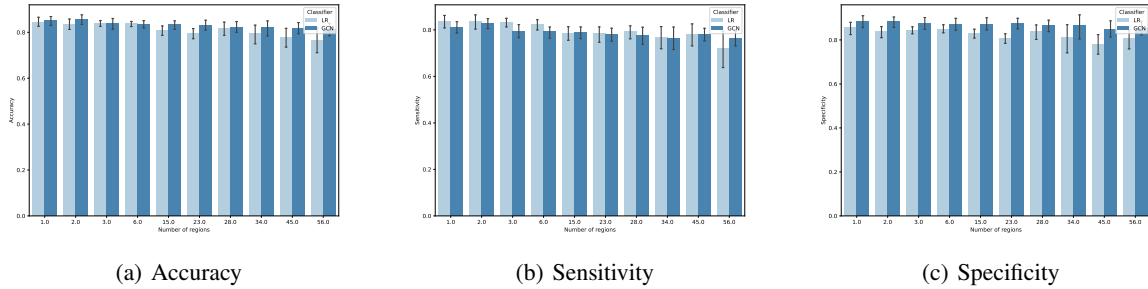


Figure 5: ABIDE I classification performance for the different numbers of brain regions selected at the graph pooling stage. Both the Logistic Regression and Graph Convolutional Networks work under the same settings.

presupposition is not only biased in the current task [16, 17, 18, 19] but also limit generalizing these methods to other brain disorder diagnosing problems. On the contrary, graph pooling requires less prior knowledge about brain functions as it straight receives the entire graph representation of brain imaging and can learn connections beyond the given brain networking. Besides, as discussed in section 2.3.2, this unsupervised downsampling method needs no training overhead. Second, it is more efficient for brain feature extraction. As shown in table 2, using features selected by graph pooling, a linear classifier can achieve much better performance than other more complex models did. In figure 5, we illustrate that the extracted features are still reliable even with the whole brain imaging downsampled to several nodes. Third, it can be aware of individual characters to some degree, which is benefited from the self-attention mechanism and sparse representation of extracted features, as discussed in section 2.3.4. We have observed differences in brain imaging pooling results of subjects from different groups, as shown in figure 4, and found even more obvious variance when we further split the groups.

3.4 Key Brain Substructures

Interpreting the ASD diagnosis framework has been being a hot topic as it may indicate the brain biomarkers of autism spectrum disorder and direct the early intervention. To intuitively exhibit the pooling results, i.e., the most critical substructures selected at that stage, we have plotted them by BrainNet Viewer proposed by [47]. We have applied graph pooling onto the brain imaging of all subjects with a pooling ratio of 0.05. Thus, for every individual, the pooling result is six selected nodes and their connections. Subsequently, we have split 871 subjects into different groups regarding their non-imaging properties, including age, gender, and the data collection site they belong to. We have surveyed the top 15 most frequently selected regions and connections from the pooling results of all subjects inside this group for each one.

Unlike figuring out universal brain biomarkers of ASD, the outputs of self-attention pooling only have specified the importance of regions and edges of individual brain imaging. However, we can still draw some conclusions by summarizing the pooling results in different groups. The illustrated substructures of the brain, as shown in figure 4, may indicate a common brain activity mechanism inside a specific group.

Ideally, as discussed in section 2.3.2, the remained regions are the first activated ones regarding external stress or active internal activities. They act like a trigger that has launched a sequence of regional activities. Based on this knowledge about model working principles, we have observed some inter-group heterogeneity in essential substructures selected by graph pooling. That finding indicates that self-attention graph pooling along can be aware of individual phenotypic properties to some degree. In figure 4, few differences have been found between ASD and Typical Control subjects as the heterogeneity caused by individual characteristics may be averaged. We further divide the two groups into four by incorporating gender into consideration, as shown in figure 6. According to the basic settings above, we may not conclude that it is the illustrated brain key substructures differences between different groups that have caused ASD.

3.5 Efficiency of Graph Convolutional Networks

In [9], the authors incorporated graph convolutional networks with brain functional selections and obtained accuracy improvement compared to [11]. The classification accuracy was increased from 66.80% to 70.40% by leveraging both imaging and non-imaging information with GCN. To figure out the efficiency of GCN in our framework, we have compared it with Logistic Regression under 10-fold cross-validation with the same dataset splits. As indicated in figure

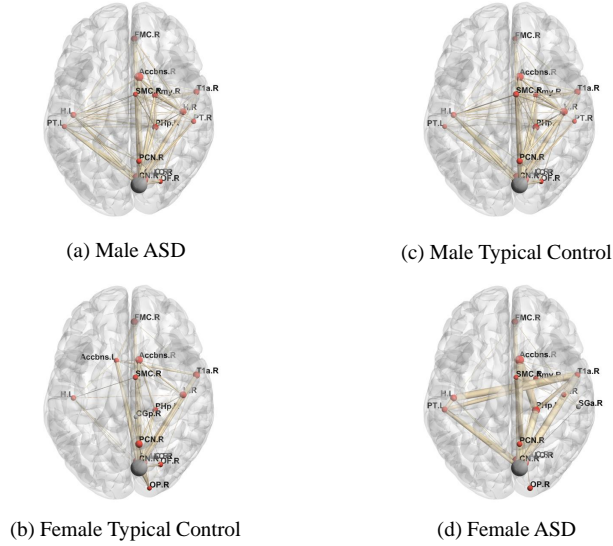


Figure 6: Additional brain view for figure 4 with same settings. The illustrated subgraphs indicate selection preference in graph pooling.

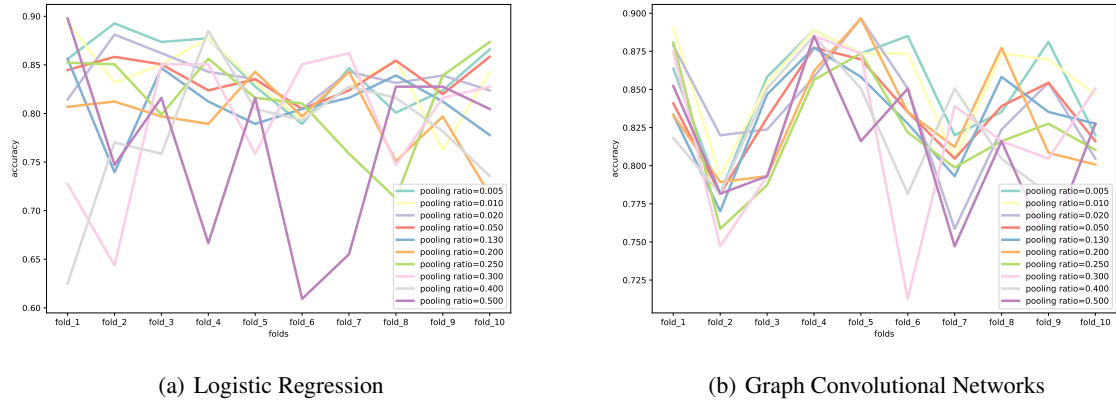
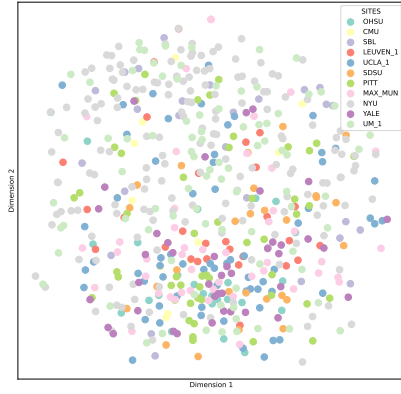


Figure 7: Impact of different folds for Logistic Regression and Graph Convolutional Networks

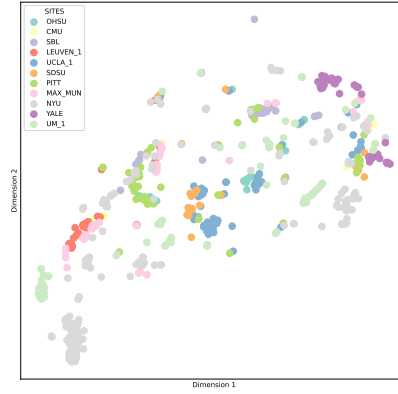
5, the two classifiers, GCN and LR, have reached the highest accuracy when the pooling ratio is set as 0.01 and 0.005, respectively. Herein, we have followed that observation and without changing other settings.

Table 4: Compare classifiers: Linear Regression and Graph Convolutional Networks. The training overhead was calculated by training the both on one fold out of 10-fold cross-validation on an NVIDIA GTX1660 TI.

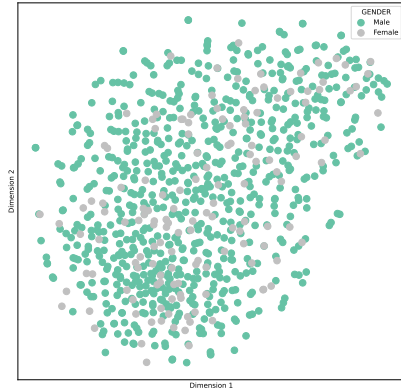
Measurement	Linear Regression	GCN
Mean Accuracy (%)	84.54	85.95
Standard Deviation of Accuracy	0.055	0.027
Area Under the ROC Curve	0.90	0.92
Standard Deviation of AUC	0.04	0.02
Average Training Overhead (s)	0.25	243.26
Average Training Epochs	625	10000



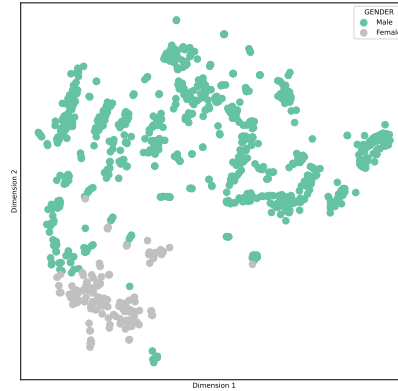
(a) Raw Extracted Features; Sites



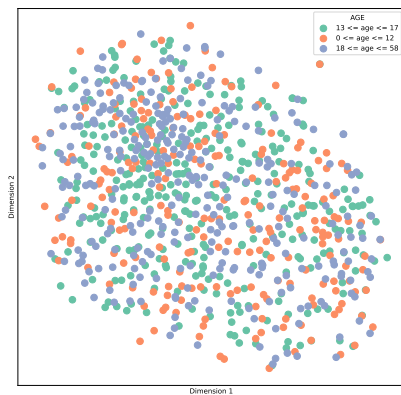
(b) Node Embeddings; Sites



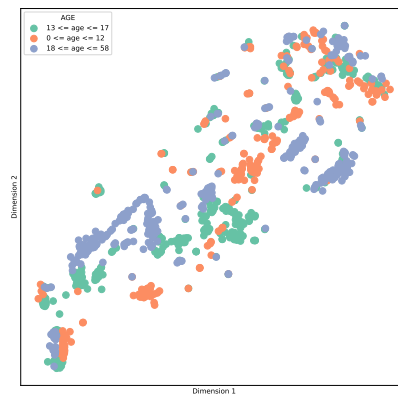
(c) Raw Extracted Features; Genders



(d) Node Embeddings; Genders



(e) Raw Extracted Features; Ages



(f) Node Embeddings; Ages

Figure 8: 2D view of the node embeddings learned by Graph Convolutional Networks. The nodes, which represent subjects, are colored according to different phenotypic properties: Sites, genders, and ages

Figure 9 indicates the classification accuracy differences between the two classifiers in terms of varied folds. Both two lines have shown the sensitivity to different training and testing datasets. To further discuss this impact of fold choice, we evaluate GCN and LR by changing graph pooling parameters. Like previously discussed, GCN should be able further to recalibrate the extracted features under the population graph. This regularization impact can be observed in figure 7, i.e., when the training and testing sets are given, the performance of GCN is more stable compared to it of logistic regression. This hypothesis is also supported by the superior of GCN concerning the standard deviation of both accuracy and AUC in table 4, which has been reported by [9, 30] as well.

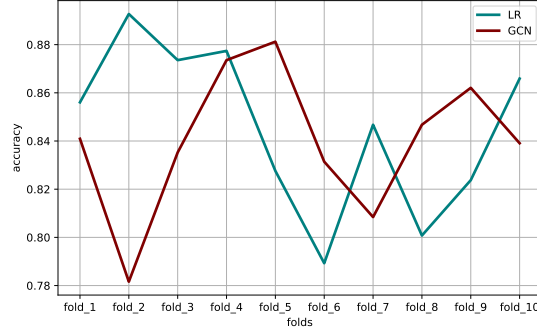


Figure 9: ABIDE I classification accuracy comparison between Linear Regression and Graph Convolutional Networks on 10 folds. Both the classifiers are trained using the same features extracted by graph pooling.

All the previous works, which have employed GCN for the same purpose of leveraging non-imaging information and fMRI [9, 30, 31], have assumed the ability of GCN to be aware of inter-individual phenotypic differences and to regularize raw features based on the former. Even though the regularization phenomenon is proved, to some degree, as discussed above, there is no clear conclusion that the GCN really has learned the inter-individual non-imaging differences. To intuitively present the learned node embeddings, we have downsampled them onto the 2D plane with t-SNE proposed by [48]. As shown in the left three plots of figure 8, even though graph pooling has detected some implicit inter-group heterogeneity, which is discussed in section 3.4, the features subsequently learned by MLP have not performed the relative feature distribution difference in respect of phenotypic information. The inevitable information loss during the feature dimensionality reduction may have caused this inconsistency, as the dimension of the basic features is up to 128. Still, the node embeddings learned by Graph Convolutional Networks have shown obvious clustering even in the 2D space. As exhibited in the right three diagrams of figure 8, the distance among subjects that are identical regarding a certain kind of phenotypic information is relatively close in the feature space compared to those who are not. This clustering is more evident when only considering the genders, which indicates that the learned edge weights of the population graph may depend more on it.

4 conclusion

In this paper, we have proposed a framework to identify Autism Spectrum Disorders. First, we have employed graph pooling to extract features directly from fMRI for the first time. This end-to-end, unsupervised, and flexible downsampling method has successfully considered brain functional connections and regional activities simultaneously. Besides, we have exploited Graph Convolutional Networks to incorporate imaging with phenotypic information and illustrated its efficiency in recalibrating the feature distribution. Our framework has achieved a mean accuracy of $85.95\% \pm 0.03$ and a mean AUC of 0.92 ± 0.02 on ABIDE I dataset. The superior performance of our model indicates its ability to detect Autism Spectrum Disorders and contribute to early intervention.

References

- [1] M. J. Maenner, K. A. Shaw, J. Baio *et al.*, “Prevalence of autism spectrum disorder among children aged 8 years—autism and developmental disabilities monitoring network, 11 sites, united states, 2016,” *MMWR Surveillance Summaries*, vol. 69, no. 4, p. 1, 2020.
- [2] L. Crane, J. W. Chester, L. Goddard, L. A. Henry, and E. Hill, “Experiences of autism diagnosis: A survey of over 1000 parents in the united kingdom,” *Autism*, vol. 20, no. 2, pp. 153–162, 2016.

- [3] H. Oba, A. Yagishita, H. Terada, A. Barkovich, K. Kutomi, T. Yamauchi, S. Furui, T. Shimizu, M. Uchigata, K. Matsumura *et al.*, “New and reliable mri diagnosis for progressive supranuclear palsy,” *Neurology*, vol. 64, no. 12, pp. 2050–2055, 2005.
- [4] M. E. Villalobos, A. Mizuno, B. C. Dahl, N. Kemmotsu, and R.-A. Müller, “Reduced functional connectivity between v1 and inferior frontal cortex associated with visuomotor performance in autism,” *Neuroimage*, vol. 25, no. 3, pp. 916–925, 2005.
- [5] N. C. Dvornek, P. Ventola, K. A. Pelphrey, and J. S. Duncan, “Identifying autism from resting-state fmri using long short-term memory networks,” in *International Workshop on Machine Learning in Medical Imaging*. Springer, 2017, pp. 362–370.
- [6] A. S. Heinsfeld, A. R. Franco, R. C. Craddock, A. Buchweitz, and F. Meneguzzi, “Identification of autism spectrum disorder using deep learning and the abide dataset,” *NeuroImage: Clinical*, vol. 17, pp. 16–23, 2018.
- [7] Z. Sherkatghanad, M. Akhondzadeh, S. Salari, M. Zomorodi-Moghadam, M. Abdar, U. R. Acharya, R. Khosrowabadi, and V. Salari, “Automated detection of autism spectrum disorder using a convolutional neural network,” *Frontiers in neuroscience*, vol. 13, p. 1325, 2020.
- [8] M. Khosla, K. Jamison, A. Kuceyeski, and M. R. Sabuncu, “3d convolutional neural networks for classification of functional connectomes,” in *Deep Learning in Medical Image Analysis and Multimodal Learning for Clinical Decision Support*. Springer, 2018, pp. 137–145.
- [9] S. Parisot, S. I. Ktena, E. Ferrante, M. Lee, R. Guerrero, B. Glocker, and D. Rueckert, “Disease prediction using graph convolutional networks: application to autism spectrum disorder and alzheimer’s disease,” *Medical image analysis*, vol. 48, pp. 117–130, 2018.
- [10] J. A. Nielsen, B. A. Zielinski, P. T. Fletcher, A. L. Alexander, N. Lange, E. D. Bigler, J. E. Lainhart, and J. S. Anderson, “Multisite functional connectivity mri classification of autism: Abide results,” *Frontiers in human neuroscience*, vol. 7, p. 599, 2013.
- [11] A. Abraham, M. P. Milham, A. Di Martino, R. C. Craddock, D. Samaras, B. Thirion, and G. Varoquaux, “Deriving reproducible biomarkers from multi-site resting-state data: An autism-based example,” *NeuroImage*, vol. 147, pp. 736–745, 2017.
- [12] A. Kazeminejad and R. C. Sotero, “The importance of anti-correlations in graph theory based classification of autism spectrum disorder,” *Frontiers in neuroscience*, vol. 14, p. 676, 2020.
- [13] S. Mostafa, L. Tang, and F.-X. Wu, “Diagnosis of autism spectrum disorder based on eigenvalues of brain networks,” *IEEE Access*, vol. 7, pp. 128 474–128 486, 2019.
- [14] Y. Wang, J. Wang, F.-X. Wu, R. Hayrat, and J. Liu, “Aimafe: autism spectrum disorder identification with multi-atlas deep feature representation and ensemble learning,” *Journal of Neuroscience Methods*, p. 108840, 2020.
- [15] J. Liu, Y. Sheng, W. Lan, R. Guo, Y. Wang, and J. Wang, “Improved asd classification using dynamic functional connectivity and multi-task feature selection,” *Pattern Recognition Letters*, vol. 138, pp. 82–87, 2020.
- [16] A. A. Sáenz, M. Septier, P. Van Schuerbeek, S. Bajiot, N. Deconinck, P. Defresne, V. Delvenne, G. Passeri, H. Raeymaekers, L. Salvesen *et al.*, “Adhd and asd: distinct brain patterns of inhibition-related activation?” *Translational psychiatry*, vol. 10, no. 1, pp. 1–10, 2020.
- [17] G. J. Harris, C. F. Chabris, J. Clark, T. Urban, I. Aharon, S. Steele, L. McGrath, K. Condouris, and H. Tager-Flusberg, “Brain activation during semantic processing in autism spectrum disorders via functional magnetic resonance imaging,” *Brain and cognition*, vol. 61, no. 1, pp. 54–68, 2006.
- [18] N. Hadjikhani, R. M. Joseph, J. Snyder, and H. Tager-Flusberg, “Abnormal activation of the social brain during face perception in autism,” *Human brain mapping*, vol. 28, no. 5, pp. 441–449, 2007.
- [19] S.-Y. Kim, U.-S. Choi, S.-Y. Park, S.-H. Oh, H.-W. Yoon, Y.-J. Koh, W.-Y. Im, J.-I. Park, D.-H. Song, K.-A. Cheon *et al.*, “Abnormal activation of the social brain network in children with autism spectrum disorder: an fmri study,” *Psychiatry investigation*, vol. 12, no. 1, p. 37, 2015.
- [20] S. I. Ktena, S. Parisot, E. Ferrante, M. Rajchl, M. Lee, B. Glocker, and D. Rueckert, “Metric learning with spectral graph convolutions on brain connectivity networks,” *NeuroImage*, vol. 169, pp. 431–442, 2018.
- [21] X. Li, N. C. Dvornek, Y. Zhou, J. Zhuang, P. Ventola, and J. S. Duncan, “Graph neural network for interpreting task-fmri biomarkers,” in *International Conference on Medical Image Computing and Computer-Assisted Intervention*. Springer, 2019, pp. 485–493.

- [22] D. Duvenaud, D. Maclaurin, J. Aguilera-Iparraguirre, R. Gómez-Bombarelli, T. Hirzel, A. Aspuru-Guzik, and R. P. Adams, “Convolutional networks on graphs for learning molecular fingerprints,” *arXiv preprint arXiv:1509.09292*, 2015.
- [23] X. Li, Y. Zhou, N. C. Dvornek, M. Zhang, J. Zhuang, P. Ventola, and J. S. Duncan, “Pooling regularized graph neural network for fmri biomarker analysis,” in *International Conference on Medical Image Computing and Computer-Assisted Intervention*. Springer, 2020, pp. 625–635.
- [24] R. Loomes, L. Hull, and W. P. L. Mandy, “What is the male-to-female ratio in autism spectrum disorder? a systematic review and meta-analysis,” *Journal of the American Academy of Child & Adolescent Psychiatry*, vol. 56, no. 6, pp. 466–474, 2017.
- [25] A. L. Rysstad and A. V. Pedersen, “There are indeed more left-handers within the autism spectrum disorder compared with in the general population, but the many mixed-handers is the more interesting finding,” *Journal of autism and developmental disorders*, vol. 48, no. 9, pp. 3253–3255, 2018.
- [26] X. Guo, K. C. Dominick, A. A. Minai, H. Li, C. A. Erickson, and L. J. Lu, “Diagnosing autism spectrum disorder from brain resting-state functional connectivity patterns using a deep neural network with a novel feature selection method,” *Frontiers in neuroscience*, vol. 11, p. 460, 2017.
- [27] Y. Kong, J. Gao, Y. Xu, Y. Pan, J. Wang, and J. Liu, “Classification of autism spectrum disorder by combining brain connectivity and deep neural network classifier,” *Neurocomputing*, vol. 324, pp. 63–68, 2019.
- [28] H. Li, N. A. Parikh, and L. He, “A novel transfer learning approach to enhance deep neural network classification of brain functional connectomes,” *Frontiers in neuroscience*, vol. 12, p. 491, 2018.
- [29] X.-a. Bi, Y. Liu, Q. Jiang, Q. Shu, Q. Sun, and J. Dai, “The diagnosis of autism spectrum disorder based on the random neural network cluster,” *Frontiers in human neuroscience*, vol. 12, p. 257, 2018.
- [30] S. Parisot, S. I. Ktena, E. Ferrante, M. Lee, R. G. Moreno, B. Glocker, and D. Rueckert, “Spectral graph convolutions for population-based disease prediction,” in *International conference on medical image computing and computer-assisted intervention*. Springer, 2017, pp. 177–185.
- [31] D. Arya, R. Olij, D. K. Gupta, A. El Gazzar, G. Wingen, M. Worring, and R. M. Thomas, “Fusing structural and functional mris using graph convolutional networks for autism classification,” in *Medical Imaging with Deep Learning*. PMLR, 2020, pp. 44–61.
- [32] Z. Rakhimberdina and T. Murata, “Linear graph convolutional model for diagnosing brain disorders,” in *International Conference on Complex Networks and Their Applications*. Springer, 2019, pp. 815–826.
- [33] A. Di Martino, C.-G. Yan, Q. Li, E. Denio, F. X. Castellanos, K. Alaerts, J. S. Anderson, M. Assaf, S. Y. Bookheimer, M. Dapretto *et al.*, “The autism brain imaging data exchange: towards a large-scale evaluation of the intrinsic brain architecture in autism,” *Molecular psychiatry*, vol. 19, no. 6, pp. 659–667, 2014.
- [34] C. Craddock, Y. Benhajali, C. Chu, F. Chouinard, A. Evans, A. Jakab, B. S. Khundrakpam, J. D. Lewis, Q. Li, M. Milham *et al.*, “The neuro bureau preprocessing initiative: open sharing of preprocessed neuroimaging data and derivatives,” *Frontiers in Neuroinformatics*, vol. 7, 2013.
- [35] R. S. Desikan, F. Ségonne, B. Fischl, B. T. Quinn, B. C. Dickerson, D. Blacker, R. L. Buckner, A. M. Dale, R. P. Maguire, B. T. Hyman *et al.*, “An automated labeling system for subdividing the human cerebral cortex on mri scans into gyral based regions of interest,” *Neuroimage*, vol. 31, no. 3, pp. 968–980, 2006.
- [36] J. M. Goldstein, L. J. Seidman, N. Makris, T. Ahern, L. M. O’Brien, V. S. Caviness Jr, D. N. Kennedy, S. V. Faraone, and M. T. Tsuang, “Hypothalamic abnormalities in schizophrenia: sex effects and genetic vulnerability,” *Biological psychiatry*, vol. 61, no. 8, pp. 935–945, 2007.
- [37] N. Makris, J. M. Goldstein, D. Kennedy, S. M. Hodge, V. S. Caviness, S. V. Faraone, M. T. Tsuang, and L. J. Seidman, “Decreased volume of left and total anterior insular lobule in schizophrenia,” *Schizophrenia research*, vol. 83, no. 2-3, pp. 155–171, 2006.
- [38] J. A. Frazier, S. Chiu, J. L. Breeze, N. Makris, N. Lange, D. N. Kennedy, M. R. Herbert, E. K. Bent, V. K. Koneru, M. E. Dieterich *et al.*, “Structural brain magnetic resonance imaging of limbic and thalamic volumes in pediatric bipolar disorder,” *American Journal of Psychiatry*, vol. 162, no. 7, pp. 1256–1265, 2005.
- [39] Z. Zhang, J. Bu, M. Ester, J. Zhang, C. Yao, Z. Yu, and C. Wang, “Hierarchical graph pooling with structure learning,” *arXiv preprint arXiv:1911.05954*, 2019.
- [40] R. Ying, J. You, C. Morris, X. Ren, W. L. Hamilton, and J. Leskovec, “Hierarchical graph representation learning with differentiable pooling,” *arXiv preprint arXiv:1806.08804*, 2018.
- [41] H. Gao and S. Ji, “Graph u-nets,” in *international conference on machine learning*. PMLR, 2019, pp. 2083–2092.

- [42] A. Martins and R. Astudillo, “From softmax to sparsemax: A sparse model of attention and multi-label classification,” in *International conference on machine learning*. PMLR, 2016, pp. 1614–1623.
- [43] T. N. Kipf and M. Welling, “Semi-supervised classification with graph convolutional networks,” *arXiv preprint arXiv:1609.02907*, 2016.
- [44] W.-L. Chiang, X. Liu, S. Si, Y. Li, S. Bengio, and C.-J. Hsieh, “Cluster-gcn: An efficient algorithm for training deep and large graph convolutional networks,” in *Proceedings of the 25th ACM SIGKDD International Conference on Knowledge Discovery & Data Mining*, 2019, pp. 257–266.
- [45] T. Eslami, V. Mirjalili, A. Fong, A. R. Laird, and F. Saeed, “Asd-diagnet: a hybrid learning approach for detection of autism spectrum disorder using fmri data,” *Frontiers in neuroinformatics*, vol. 13, p. 70, 2019.
- [46] H. Jiang, P. Cao, M. Xu, J. Yang, and O. Zaiane, “Hi-gcn: A hierarchical graph convolution network for graph embedding learning of brain network and brain disorders prediction,” *Computers in Biology and Medicine*, vol. 127, p. 104096, 2020.
- [47] M. Xia, J. Wang, and Y. He, “Brainnet viewer: a network visualization tool for human brain connectomics,” *PloS one*, vol. 8, no. 7, p. e68910, 2013.
- [48] L. Van der Maaten and G. Hinton, “Visualizing data using t-sne.” *Journal of machine learning research*, vol. 9, no. 11, 2008.